GEOPHYSICS, VOL. 63, NO. 5 (SEPTEMBER-OCTOBER 1998); P. 1685—1695, 8 FIGS.

Elastic reverse time migration of marine walkaway vertical seismic profiling data

Ketil Hokstad*, Rune Mittet‡, and Martin Landrø**

ABSTRACT

Walkaway vertical seismic profiling (VSP) acquisition with three-component geophones allows for direct measurement of compressional as well as shear energy. This makes full elastic reverse time migration an attractive alternative for imaging data.

We present results from elastic reverse time migration of a marine walkaway VSP acquired offshore Norway. The reverse time migration scheme is based on a high-order finite-difference solution to the two-way elastic wave equation. Depth images of the subsurface are constructed by correlation of forward- and back-propagated elastic wavefields. In the walkaway VSP configuration, the number of shots is much larger than the number of geophone levels. Using processing methods operating in the shot/receiver domain, it is advantageous to use the reciprocal relationship between the walkaway VSP and the reverse VSP configurations. We do this by imaging each component of each geophone level as a reverse VSP common shot gather. The final images are constructed by stacking partial images from each level.

The depth images obtained from the vertical components reveal the major characteristics of the geological structure below geophone depth. A graben in the base Cretaceous unconformity and a faulted coal layer can be identified. The horizontal components are more difficult to image. Compared to the vertical components, the horizontal component images are more corrupted by migration artifacts. This is because the horizontal component images are more sensitive to aperture effects and to the shear-wave velocity macromodel. When converted to two-way time, the migration results tie well with the surface seismic section.

Comparison of fully elastic and acoustic reverse time migration shows that the vertical component is dominantly *PP*-reflected events, whereas the horizontal components get important contributions from *PS*-converted energy. The horizontal components also provide higher resolution because of the shorter wavelength of the shear waves.

INTRODUCTION

In a 2-D walkaway vertical seismic profiling (VSP) survey, a moving source is fired at typically 200 positions along the survey line, and data are recorded at a few depth levels with stationary downhole geophones. For migration schemes where the modeling of each shot is part of the migration process, and for other processing algorithms operating in the shot-receiver domain, the large number of shots is a problem. Using such types of algorithms, reverse VSP data, acquired with a downhole source, can be processed much more efficiently.

The walkaway VSP and reverse VSP configurations are linked through the principle of reciprocity. If the variations in the source signal from shot to shot are small, a walkaway VSP experiment can be transformed into the reverse VSP configuration for processing purposes. Marine walkaway VSP data are usually acquired with small air-gun arrays with approximately spherical radiation characteristics for seismic wavelengths, and three components of displacement velocity are measured at the geophone. A reciprocity relation, which accounts for directivity characteristics at the source and receiver side and which is valid in the fully elastic case, has been presented by Mittet and Hokstad (1995). This relation forms a theoretical basis for the application of reciprocity in marine walkaway VSP processing.

In this paper, we present the results from 2-D elastic reverse time migration of a marine walkaway VSP data set from the

Manuscript received by the Editor November 8, 1996; revised manuscript received December 19, 1997.
*IKU Petroleum Research, N-7034 Trondheim, Norway, and Norwegian University of Science and Technology, N-7034 Trondheim, Norway; E-mail: ketil.hokstad@iku.sintef.no.
‡Formerly IKU Petroleum Research; presently Sting Research, Rosenborg Gt. 17, N-7014 Trondheim, Norway; E-mail: konrumi@statoil.no.
**Formerly IKU Petroleum Research; presently Statoil Research Centre Postuttak, N-7005 Trondheim, Norway; E-mail: mlan@statoil.no.

North Sea. The geology below the walkaway VSP line is relatively simple in the crossline direction. Therefore the data set is well suited for 2-D data processing.

The reverse time migration scheme is founded on nonlinear inversion theory (Tarantola, 1984; Mora, 1987; Mittet et al., 1994). It is based on a coarse-grid, finite-difference solution to the two-way, isotropic, elastic wave equation (Holberg, 1987; Mittet et al., 1988). We construct depth images of the subsurface by displaying elastic gradients that are computed by correlating forward-propagated fields with back-propagated residual fields. This imaging condition is equivalent to Claerbout's (1971) principle. Because the migration scheme is fully elastic, we do not need to separate *P*- and *S*-waves. We avoid the simplifying assumptions regarding the earth, which underlie most methods for accomplishing this. Reverse time migration of reverse VSP data has been presented by Chen and McMechan (1991, 1992).

One of the motivations for performing the work presented here was to test processing methods and algorithms before extending the methodology to 3-D. The first results from application of the scheme to real 3-D walk-away VSP data have been presented by Mittet et al. (1997b).

DATA ACQUISITION

The walkaway VSP data were acquired in a slightly deviated well offshore Norway in 1992. The deviated well coincides with a vertical well for the upper 2000 m. Two walkaway VSP lines running approximately east–west were acquired. The total length of the lines was 4.9 and 6.0 km, respectively. The seismic source was a cluster of 3×200 in.^{3} air guns. The geophones were located approximately 3.0 km below mean sea level. For each of the lines, data were recorded with a five-shuttle, three-component tool, giving ten common geophone gathers. The bottom common geophone gather (level 1) was corrupted by noise and was discarded in the processing.

APPLICATION OF RECIPROCITY IN WALKAWAY VSP PROCESSING

The walkaway VSP and reverse VSP configurations are linked by the principle of reciprocity. For the scalar wave equation, the application of reciprocity is straightforward: Source and receiver positions can be interchanged without changing the wavefield. In a marine walkaway VSP experiment, sources with an approximately spherical symmetry are fired in the water layer and displacement velocity, which is a vector quantity, is recorded with multicomponent geophones. The reciprocity equation relating the walkaway VSP and reverse VSP configurations must properly account for the directivity properties on the source as well as the receiver side.

For the general elastic case, Mittet and Hokstad (1995) show that the reciprocity transformation relating displacement velocity v_i measured in a walkaway VSP experiment to pseudo-pressure $\dot{\Psi}$ measured in a reverse VSP can be expressed as

$$\dot{\Psi}(\mathbf{x}_s|\mathbf{x}_g, t; e_i) = -M(\mathbf{x}_s)\, v_i(\mathbf{x}_g|\mathbf{x}_s, t) e_i, \qquad (1)$$

where $i = x, y,$ or z; $M(\mathbf{x}_s)$ is the bulk modulus in water; and $v_i(\mathbf{x}_g|\mathbf{x}_s, t)$ is the i-component of the elastic displacement velocity vector recorded in a marine walkaway VSP with a monopole source located at $\mathbf{x}_s$ in the water layer. The value $\dot{\Psi}(\mathbf{x}_s|\mathbf{x}_g, t; e_i)$ is the acoustic pseudo-pressure recorded at $\mathbf{x}_s$ in a marine reverse VSP experiment with a directive source in the direction of the unit vector e_i located at $\mathbf{x}_g$ in an elastic subsurface. The dot above Ψ denotes differentiation with respect to time. Synthetic tests have shown that this reciprocity relation is very accurate for both traveltimes and amplitudes.

From a practical point of view, the elastic reciprocity transformation is very simple. It amounts to a reinterpretation of the WVSP common receiver gathers as RVSP common shot gathers for each component of the displacement vector. Simultaneously, the source contribution is changed from spherically symmetric to directional.

In walkaway VSP modeling and processing using an acoustic wave equation, the directional sources should be interpreted as dipole source distributions because true directional body forces can be generated only when the shear modulus is not zero.

PREPROCESSING

Figure 1 shows the processing sequence applied to image the walkaway VSP data. The processing sequence is relatively simple and deviates from standard practice in the industry. Therefore, we will discuss the various steps of the sequence. In view of the reciprocity relation given above, we shall interchangeably speak of the data set as walkaway VSP or reverse VSP data,

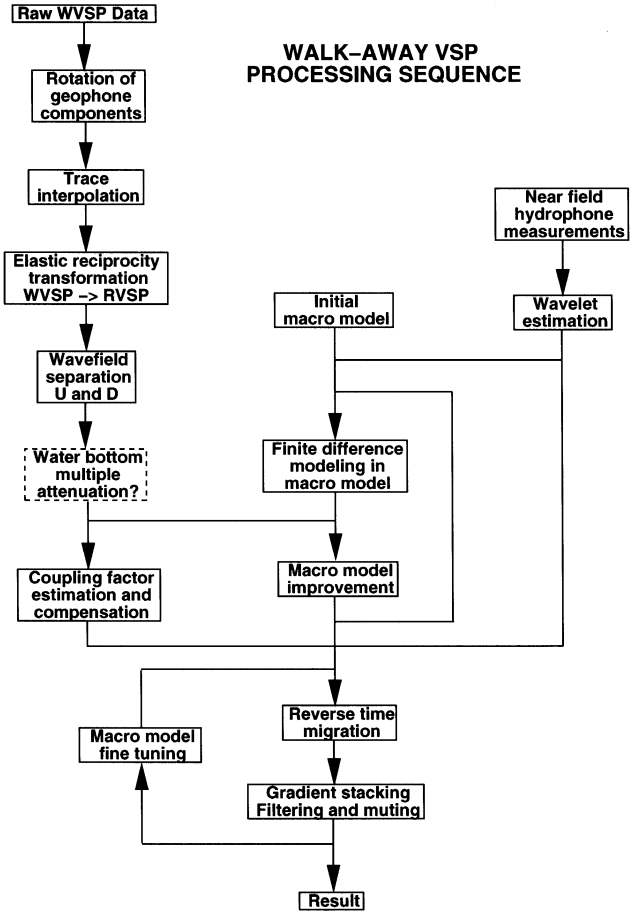

FIG. 1. Walkaway VSP processing sequence.

depending on the most convenient configuration for each processing step.

Rotation of geophone components

The local deviation angle of the well at geophone depth is approximately 10°, and the acute angle between the survey line and the projection of the well onto the horizontal plane is approximately 25°. Using the iterative method presented by Hokstad (1995), we estimated the orientation of the geophone axis for each shot in the survey. In the walkaway VSP configuration, the geophone is stationary in the well for all shots along the survey line. If the main assumption of the angle estimation scheme—lateral invariance of the subsurface in the cross-line direction—is fulfilled, the computed rotation angles will be equal for all shots. For the real walkaway VSP data, we found slight variations from shot to shot. For each geophone level, the estimated angles were averaged over the shots, excluding the small offsets. Using the estimated angles, we rotated the geophone components into alignment with a reference frame defined by the in-line direction and the vertical.

Water bottom multiple attenuation

The removal of all types of free surface multiples, without making any assumptions about horizontal layering, is a demanding task. A method for accomplishing this in the general elastic case has been developed (Fokkema and Van den Berg, 1990; Wapenaar et al., 1990). This method, however, is not applicable to walkaway or reverse VSP data because it requires full reciprocity in the data set, i.e., each receiver position must be a source position at least once. A less ambitious and more realistic goal is to attenuate the multiple reflections generated by the free surface and the water bottom, which are the most important because of the usually relatively large reflection coefficient of the water bottom. To achieve this, we have adapted a scheme proposed by Wiggins (1988) to be applicable to walkaway VSP data.

The water-bottom multiple attenuation scheme is formulated according to the reverse VSP configuration. First, we separate each reverse VSP common shot gather into up- and down-going waves right below the air–water surface. The wavefield separation is performed in the frequency-wavenumber domain. In the walkaway VSP configuration, this amounts to a source deghosting. Second, we extrapolate the common shot gathers down to the water bottom with the Kirchhoff integral. Third, the water-bottom multiples are predicted and subtracted from the data. The multiple reflections are computed by convolving the down-going waves with a short spatial and temporal convolution operator that approximates the water-bottom reflectivity. The convolution operator is linear and can be computed by solving a least-squares optimization problem, equivalent to the design of a Wiener filter. We used convolution operators where the half-lengths in the space and time directions were $L_x = 2$ and $L_t = 8$, respectively. Finally, the up-going wavefield is extrapolated back to hydrophone depth. At the final step, the data can be extrapolated to the finite-difference grid.

For our walkaway VSP data set, the air-gun bubble period and the water-bottom multiple period are close to equal, which means bubble oscillations and multiple reflections interfere in time. A weakness of Wiggins' method is that it is not fully effective when events in the data interfere.

Trace interpolation

The spatial sampling of the raw common geophone gathers was highly irregular. The average trace spacing was 29 and 34 m for the two passes with the vessel, respectively. The shot interval varied from a maximum of 160 m (pass 1) and 240 m (pass 2) at zero offset, where the rig interfered with the vessel, down to a minimum of 7 m. In a migration scheme where the wave propagation is based on finite differences, the velocity and density macromodel is discretized on a regular grid. The data must be interpolated to coincide with the nodes of the grid.

The irregular spatial sampling of the data excludes most interpolation algorithms working in the Fourier or τ–p domains. We tested two different interpolation methods: pure cubic spline interpolation and a combination of cubic splines and interpolation with the Kirchhoff integral. The spline interpolation was done in two steps. First, we interpolated across the zero-offset gap to a trace interval approximately equal to the average trace interval. In this step, we low-pass filtered a copy of the data, with the high-cut wavenumber defined by the size of the gap, and interpolated using only the low wavenumber part of the spectrum. The interpolated traces were then merged into the gap in the unfiltered data. Second, we interpolated the resulting data to a regular trace spacing of 12.5 m. To enhance the performance of the spline interpolation, we applied a simple constant-velocity NMO to flatten major events before interpolation. After interpolation, the NMO was removed.

When performing trace interpolation with the Kirchhoff integral, the second spline interpolation step was replaced by wavefield extrapolation using the Kirchhoff integral. With this approach, the trace interpolation can be integrated with the multiple attenuation method discussed in the previous subsection. At the final step of the multiple attenuation algorithm, the wavefield is extrapolated from the water bottom back to hydrophone depth. We can then extrapolate the wavefield to spatial locations coinciding with the regular grid.

From a theoretical point of view, interpolation with the Kirchhoff integral is the more attractive method because it is based on the acoustic wave equation. Cubic splines are a purely mathematical device; when using splines to interpolate seismic data, we make some assumptions that are not always valid. We have, however, experienced in tests with both real and synthetic data that the combined process of trace interpolation and migration is very stable and that the choice between the two methods is unimportant.

Coupling factor estimation and compensation

During acquisition of a walkaway VSP, the coupling between the well and the tool may change and the source characteristics can vary slightly from shot to shot. This should be compensated for in the data processing. When the wave propagation is governed by a linear wave equation, the effects of the well-tool coupling and the amplitude variations of the source can be combined into effective coupling factors. In the case of real data, the effective coupling factors also give approximate compensation for various effects not accounted for elsewhere in

the processing, such as the amplitude loss attributable to absorption and 3-D geometrical spreading for the first arrival.

For each trace in a gather, we define the effective coupling factor as the ratio of the rms energy in real and synthetic data:

$$a_i^{\mathrm{rms}}(\mathbf{x}) = \sqrt{\frac{\int dt\left[v_i^{\mathrm{obs}}(\mathbf{x}_g, t)\right]^2}{\int dt\left[v_i^{\mathrm{mod}}(\mathbf{x}_g, t)\right]^2}}. \qquad (2)$$

Here, $v_i^{\mathrm{obs}}(\mathbf{x}, t)$ and $v_i^{\mathrm{mod}}(\mathbf{x}_g, t)$ are measured and modeled components of displacement velocity. The synthetic data were modeled in a smooth macrovelocity model. Compensation for the effective coupling factors is achieved by multiplying each trace by the inverse of equation (2).

3-D geometrical spreading correction

A single real walkaway VSP line is an experiment with 2-D measurement and 3-D wave propagation. The wave propagation in the reverse time migration scheme is 2-D, as is the implementation of the preprocessing algorithms that we used. The 3-D geometrical spreading in the real data should be accounted for in the processing. The 3-D to 2-D geometrical spreading correction can be applied accurately only for horizontally layered media and data sets with cylinder symmetry. In the case of real data, such an assumption will be violated. For a split-spread walkaway VSP data set, the cylinder symmetrical assumption introduces additional difficulties because contributions from negative offsets are wrapped over to the positive offsets, and vice versa. We tried to use the geometrical spreading correction presented by Amundsen (1993), treating positive and negative offsets separately. This method, however, was rejected because the cylinder symmetry assumption introduced spatial discontinuity in the data at zero offset and because the data became too corrupted by aperture effects. We ended up using no correction for 3-D effects other than what we obtained through the compensation for effective coupling factors. This seems to be sufficient, though not optimal, for walkaway VSP imaging over a wide range of offsets and arrival times.

Source wavelet estimation

In standard VSP processing, spiking or waveshaping deconvolution is usually applied to the data to remove the source signature from the data. We have taken another approach—namely, to model the full waveform in the data as part of the migration process.

The RTM scheme we use requires an estimate of the source time function of the air-gun cluster as input. To estimate the source time function, including air-gun bubble oscillations, we used a source modeling program that solves a modified Kirkwood–Bethe equation (Landrø and Sollie, 1992). Near-field measurements of the cluster were used to calibrate the source modeling. To account for the pulse modification during propagation from absorption, we applied a filter to the wavelet. This filter was designed so we got a reasonably good fit between the waveforms in the modeled and measured first arrivals of the walkaway VSP data set.

MACROMODEL CONSTRUCTION

A major concern in seismic depth migration is the construction of good density and velocity macromodels. For walkaway VSP data, the standard velocity analysis methods used with surface seismic data are not directly applicable. The macromodel we used in the walkaway VSP migration is a synthesis of information obtained in various ways. We started from a model suggested by the contractor who had processed this data set. The contractor's P-wave velocity and density models were defined by identifying the log responses at formation boundaries on the calibrated sonic log. The geometry of the model away from the well was based on surface seismic data in the area. The S-wave velocity model was computed from the P-wave velocity model using a constant v_P/v_S-ratio of 1.7.

We performed a few finite-difference forward modeling operations in the macromodel. After each modeling operation, the upper part of the P-wave velocity profile (above the geophones) was modified systematically to give a gradually better match between first-arrival traveltimes in real and modeled data. To compensate empirically for P-wave anisotropy, a plane layer in the overburden was replaced by a laterally variant syncline-shaped layer, thereby reducing the traveltime of rays arriving at large offsets.

The iteration-by-hand procedure outlined above is less applicable for adjusting the S-wave model and the P-wave model below the geophones. To improve this part of the model, we incorporated P- and S-wave velocities which had been estimated by G. Jackson (formerly at Elf UK) using the WishingWell software.

When choosing the node spacing in the finite-difference grid, the frequency content in the data and the minimum nonzero velocity in the macromodel must be taken into account. This is necessary to avoid significant numerical dispersion in the wave propagation. With a maximum frequency of approximately 70 Hz, the node spacing in the x- and z-directions was set to $\Delta x = 12.5$ m and $\Delta z = 6.25$ m. Before the reverse time migration, we filtered the macromodel below the water bottom to get smooth density and velocity profiles. The water bottom was not smoothed to preserve the discontinuity at the liquid–solid interface. The spatial low-pass filter removes information above 10% of the Nyquist wavenumber. The filter operates on slowness to preserve the traveltimes. To simulate a water layer extending to infinity in the negative z-direction, we put an absorbing buffer with a width of 30 grid points at the top of the macromodel.

REVERSE TIME MIGRATION

The walkaway VSP data were imaged using a fully elastic reverse time migration scheme, which is based on nonlinear inversion theory (Tarantola, 1984; Mora, 1987; Mittet et al., 1994; Mittet et al., 1997a). The mathematical details are given in the Appendix. Using an elastic migration scheme, P- and S-energy is imaged in a single step, and no P/S-separation is required in preprocessing the data. In the migration of the walkaway VSP data, we use the reciprocal relationship between the walkaway and reverse VSP configurations: each component of displacement velocity is processed as reverse VSP pseudo-pressures as defined in equation (1). The vertical and horizontal components are imaged separately.

Migration consists of two steps: wavefield extrapolation and imaging. We perform wavefield extrapolation, forward and backward in time, by a high-order finite-difference solution to the two-way elastic wave equation. The scheme is second order in time, and spatial derivatives are computed by the high-order operators proposed by Holberg (1987). The operator half-lengths in the x- and z-directions were $L_x = L_z = 8$.

The elastic depth images are constructed by displaying the gradients of the density and Lamé parameters λ and μ. The gradients are computed by correlation of forward- and backward-modeled wavefields as shown in equations (A-4) and (A-5). When the wavefield extrapolation is performed in a smooth macromodel, this imaging condition becomes equivalent to Claerbout's U/D principle (Claerbout, 1971). To improve the S/N ratio, the partial images from each shot are stacked to give the final image. The gradient with respect to the Lamé parameter λ is constructed from local P-energy only and is denoted P-image in the following. The density gradient generally gets contributions from both local P- and S-energy. It is sensitive to both PP-reflections and PS-conversions on the reflectors. It is called $P\&S$-image in the following. The gradient with respect to μ duplicates the information in the density gradient and is not shown.

Figure 2 shows the surface seismic section for the area of interest. Two major reflectors are present within the zone covered by the walkaway VSP survey: the base Cretaceous

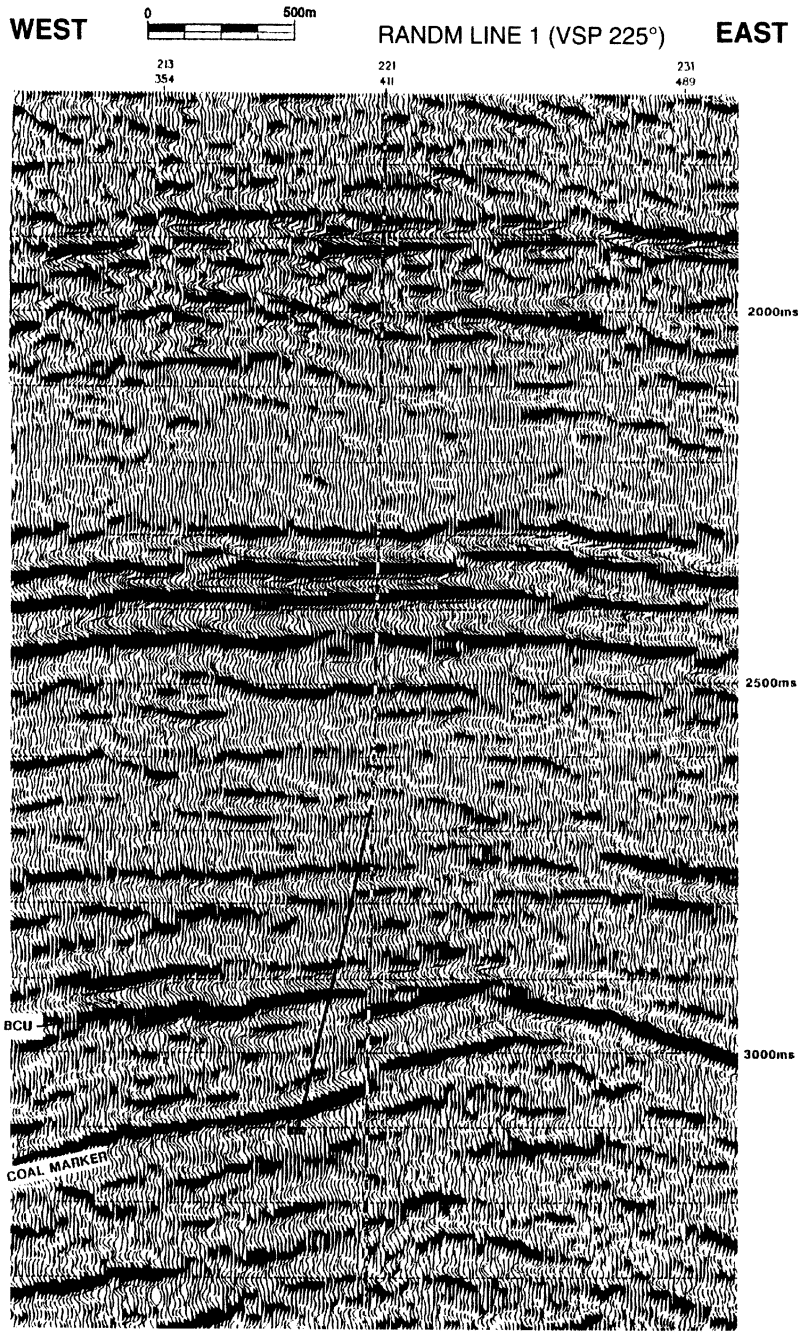

FIG. 2. Surface seismic section from the area of interest. The solid line is the well.

unconformity is found immediately below 2.9 s two-way time, and a dipping coal marker intersects the well between 3.0 and 3.1 s two-way time. The coal marker is faulted, with a fault plane intersecting the well at approximately 3700 m. A Jurassic reservoir is located between the base Cretaceous unconformity and the coal layer.

Elastic reverse time migration

Figure 3 shows the P- and P&S-images obtained from the z-component of a single geophone level (level 8). The reference frame is relative to the wellhead. Figure 4 shows the images obtained by stacking the partial images obtained from the z-components at all nine levels. On the elastic z-component images, we can identify the base Cretaceous unconformity at 3.6 km, with a graben starting at approximately $x \simeq 0$. The dipping reflector at 3.8 km is the coal marker. The coal marker is faulted, with the fault plane intersecting the well at approximately 3.7 km. Below the coal marker, at the right side of the well, the geology is probably complex, and there may be additional faults in this region. Comparing Figures 3 and 4, we observe the images are improved by using all available geophone levels when imaging the walkaway VSP data. The S/N ratio is improved by stacking the partial images. Coherent events add constructively, whereas artifacts and random noise are attenuated.

The x-components are more difficult to image because they are very sensitive to the S-wave velocity model and finite aperture. Figure 5 shows the P- and P&S-images obtained by stacking the x-component partial images from all geophone levels. Compared to the z-component, the x-component images are more corrupted by migration smiles and artifacts. The base Cretaceous unconformity and the coal marker can, however, be recognized.

To compare the walkaway VSP images with the surface seismic section (Figure 2), we transformed the P&S-images from the x- and z-components to two-way traveltime using the P-wave velocity macromodel. Figures 6 and 7 show the P&S-images (Figures 4 and 5) transformed to two-way time and merged into the surface seismic section. The walkaway VSP images tie well with major reflectors at the surface seismics.

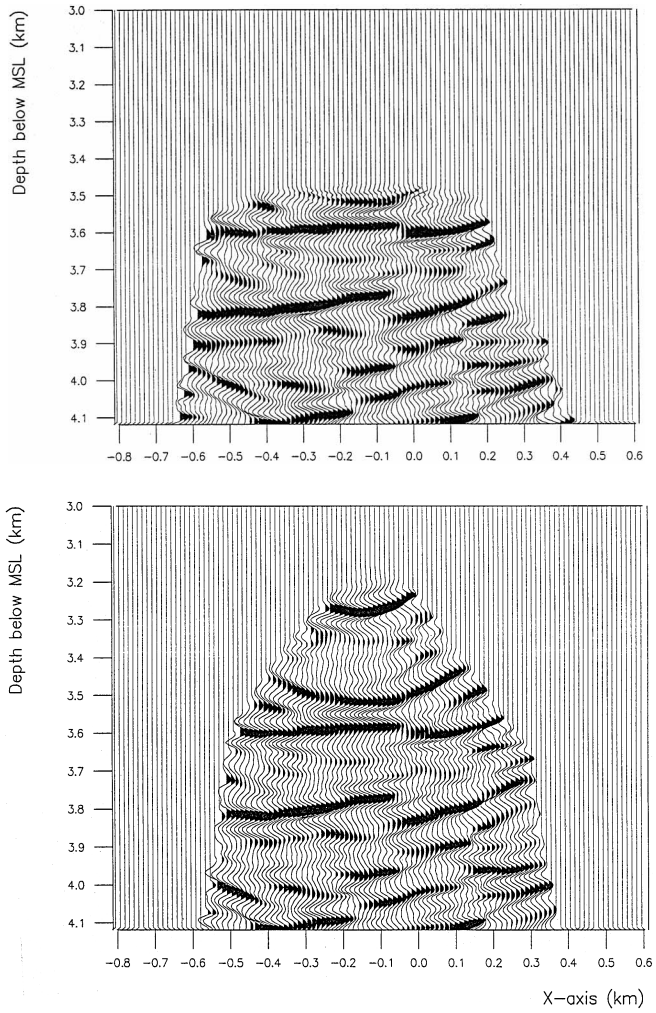

FIG. 3. Elastic reverse time migration of a single z-component (level 8) for (a) P-image and (b) P&S-image.

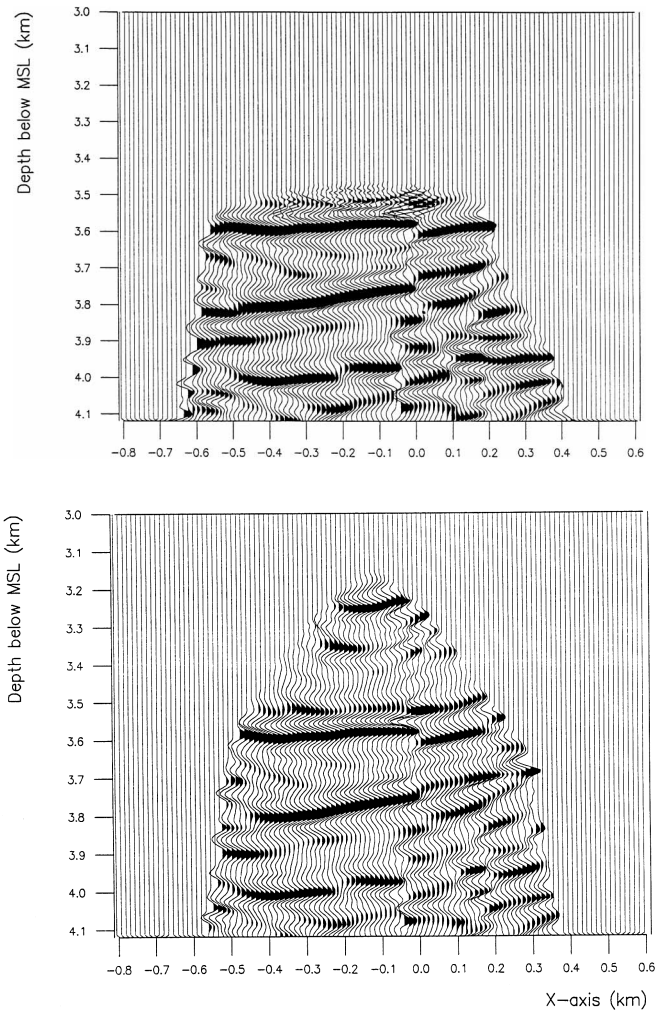

FIG. 4. Elastic reverse time migration of nine z-components for (a) P-image and (b) P&S-image.

Acoustic reverse time migration

For comparison, the walkaway VSP data were migrated using an acoustic macromodel as well, setting the *S*-wave velocities to zero. The result from acoustic reverse time migration of the *z*-components is shown in Figure 8. Comparing with Figure 4, we observe that, for the *z*-components, the result is not significantly degraded by migration in the acoustic approximation.

Acoustic migration of the *x*-components gives meaningless results, as expected, because the *x*-components contains considerable amounts of *PS*-conversions.

DISCUSSION

The *P*-images are obtained by correlating local *P*-energy at each node of the finite-difference grid within the region of interest. Correspondingly, the *P*&*S*-images are in general obtained by correlating both local *P*- and *S*-energy. The surface seismics (Figure 2) indicate the overburden is close to plane layered and the target zone for the walkaway VSP survey consists of possibly faulted but otherwise small dipping layers. Fault-plane reflections fall outside the aperture of the walkaway VSP experiment. Therefore, it is reasonable to suspect that the *z*-components of the walkaway VSP data are dominated by *PP*-reflections recorded at small and intermediate offsets. *PS*-converted energy propagating at large angles from the vertical give minor contributions to the *z*-components. This is confirmed by the images obtained by acoustic reverse time migration. From a reverse VSP point of view, this can be understood from the radiation characteristics of directional sources. With a force in the *z*-direction, *P*-energy is radiated within a fan around the vertical axis, whereas *S*-energy is radiated within a fan around the *x*-axis.

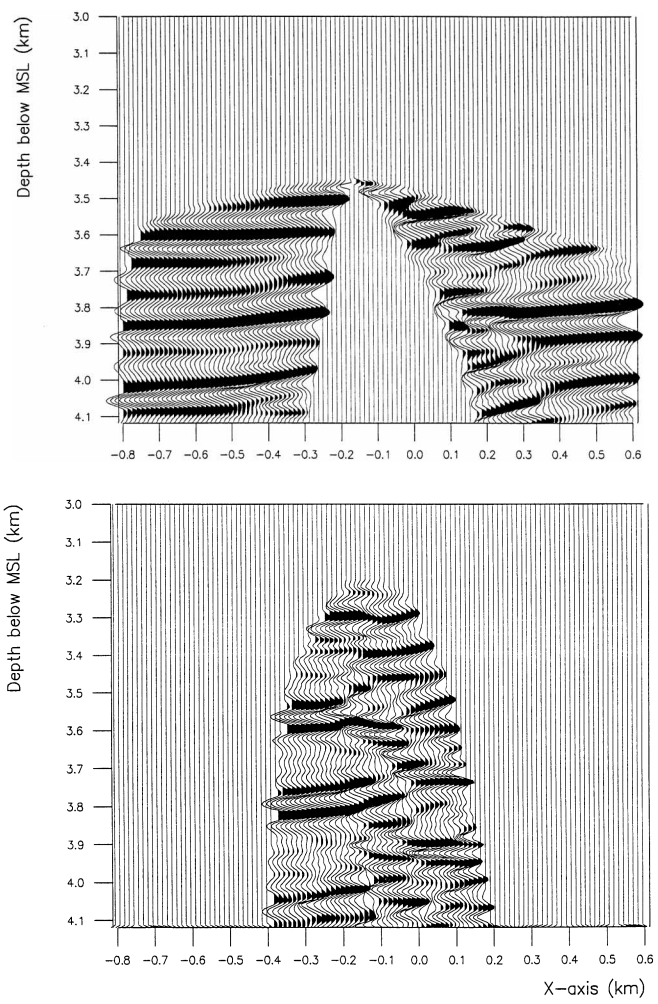

FIG. 5. Elastic reverse time migration of nine *x*-components. (Top) *P*-image; (bottom) *P*&*S*-image.

The *P*- and *P*&*S*-images obtained from the *x*-components are nearly complementary. This also may be understood from the radiation characteristics of direction forces. For a reverse VSP shot with a force in the *x*-direction, *P*-energy is radiated near the horizontal plane, whereas *S*-energy is radiated near the vertical direction. Consequently, the *x*-component receives *PS*-conversions at small offsets and *PP*-reflections at large offsets. The *PP* image from the *x*-component vanishes at small offsets, as do the *PP* reflected and transmitted waves on the *x*-component in walkaway VSP data. The *S*-waves have lower velocity and shorter wavelength than the *P*-waves. Therefore, *PS*-converted energy may resolve detail on a smaller scale near the well. Comparing the *x*- and *z*-component images (e.g., Figures 6 and 7), we see this is the case.

CONCLUSIONS

We have presented the results obtained from elastic reverse time migration of marine walkaway VSP data. In the area where the walkaway VSP survey was completed, the geology is fairly simple in the cross-line direction. Therefore, it is possible to obtain good results from 2-D processing.

We imaged the *x*- and *z*-components separately by using the reciprocal relationship between the walkaway and reverse VSP configurations. The depth images obtained from the *z*-components reveal the major characteristics of the geological structure below geophone depth. The base Cretaceous unconformity with a graben at 3.6 km depth and the faulted coal marker at 3.8 km can be identified on the *z*-component images. After transformation to the two-way time domain, the elastic images tie well with the surface seismic section. A numerical test using acoustic reverse time migration showed that the *z*-component images were not significantly degraded by acoustic approximation. This indicates the events recorded on the *z*-components are dominantly *PP*-reflections.

Compared to the *z*-component images, the images obtained from the *x*-component are more corrupted by migration smiles and artifacts. However, when interpreted together with the *z*-component images, they provide some information. On the *x*-component *P*-images, continuous reflectors are imaged farther away from the well. The *x*-component *P*&*S*-images get important contributions from *PS*-converted energy recorded at small offsets, resolving details near the well. The *x*-component images are sensitive to the *S*-wave velocity macromodel below geophone depth.

Currently, we are working on 3-D elastic RTM of a 3-D marine WVSP. The real data example presented in this paper demonstrates that full elastic RTM is an attractive alternative for imaging of WVSP data, and that both *P*- and *S*-energy can be used in the construction of the depth images.

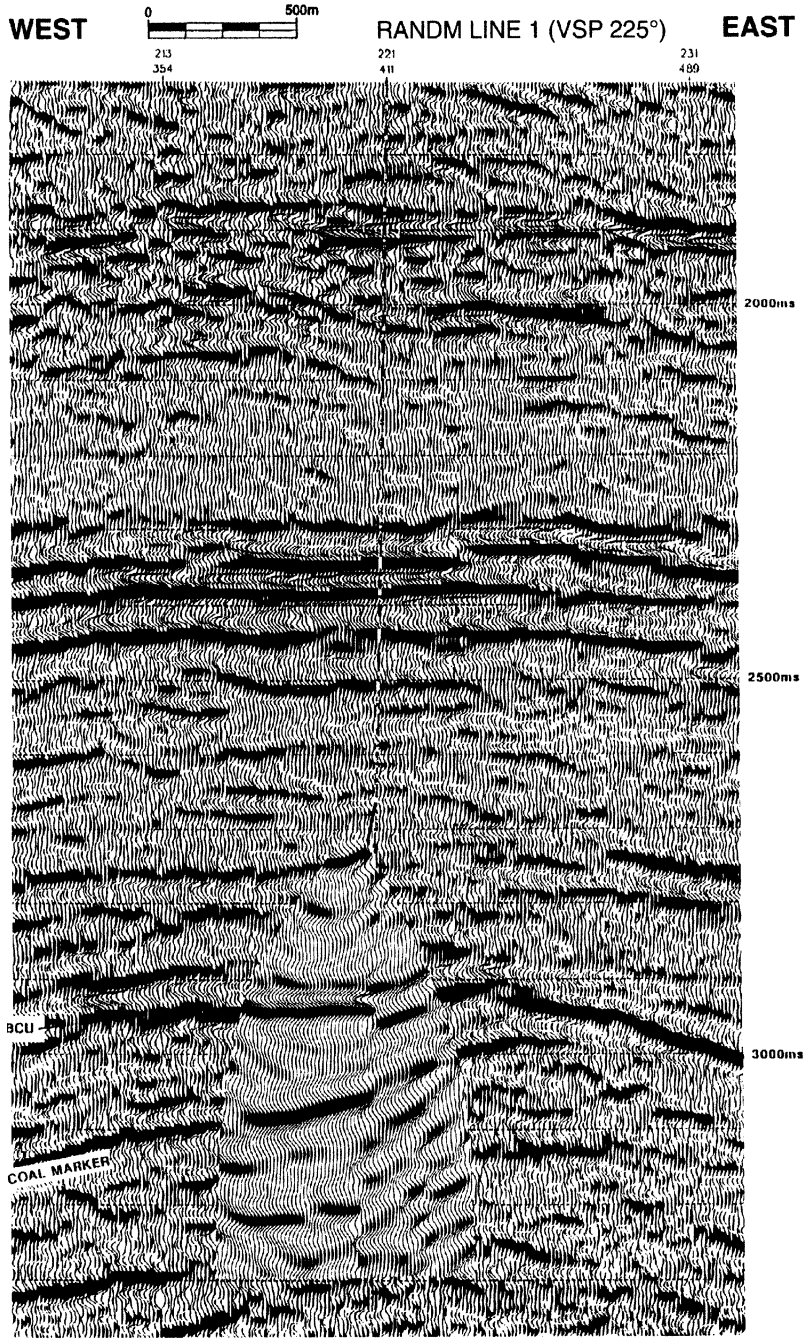

FIG. 6. Elastic reverse time migration of nine *z*-components. The *P*&*S* depth image is transformed to two-way traveltime and merged into the surface seismic section.

ACKNOWLEDGMENTS

We thank the participants of the 3-D VSP project, Elf Petroleum Norge AS, Norsk Agip A/S, Norsk Hydro a.s., Norwegian Petroleum Directorate, Statoil and TOTAL Norge A.S., for financial support and for permission to publish the results. Furthermore, we thank Lasse Amundsen (Statoil), Eivind Berg (S&B Geophysical, formerly Statoil), Arild Haugen (NPD), Philippe Julien (TOTAL), Peter Macalister-Hall (TOTAL), Jean-Marc Mougenot (Elf), and Steen Petersen (Norsk Hydro) for discussions. We thank Elf Petroleum Norge a.s., for permission to use the real data, and we are grateful to Geoffrey Jackson, formerly of Elf Geoscience Research Centre, for giving us the results from his velocity analysis.

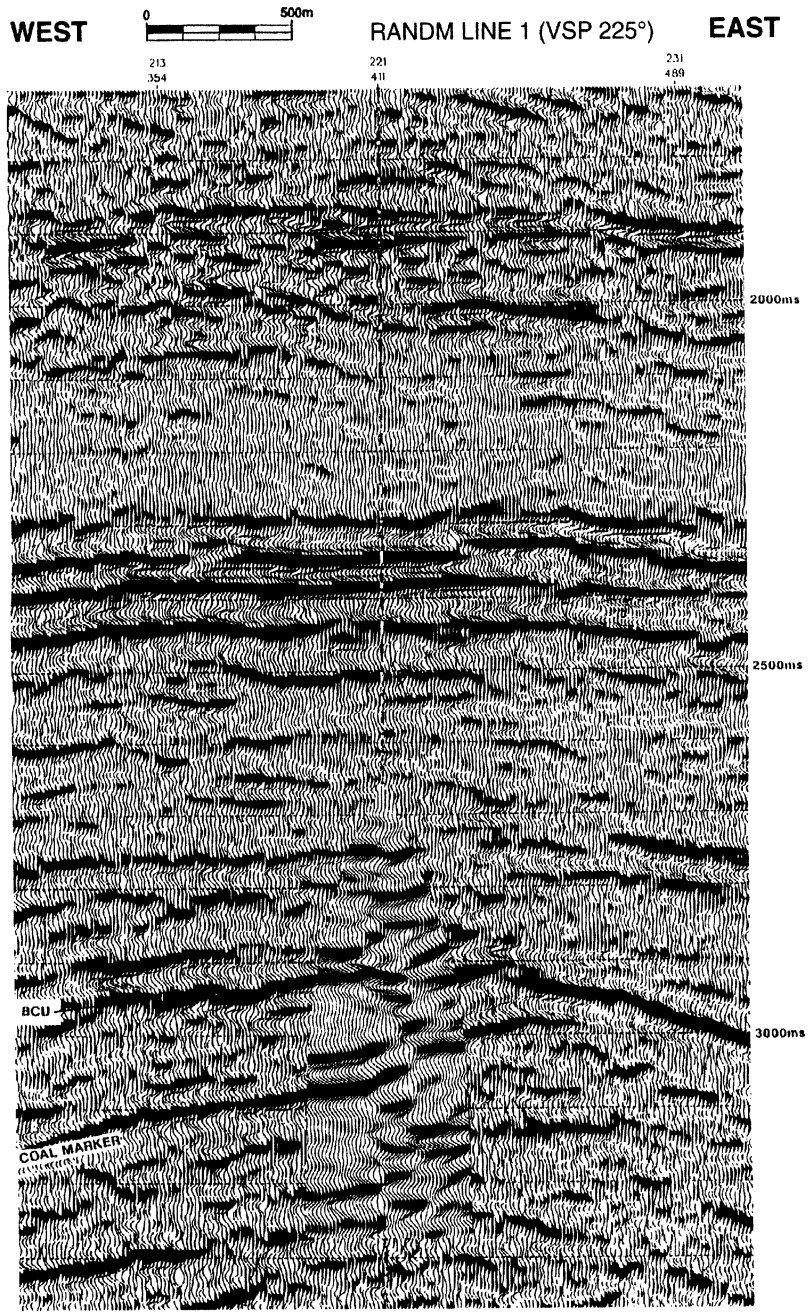

FIG. 7. Elastic reverse time migration of nine *x*-components. The *P*&*S* depth image is transformed to two-way traveltime and merged into the surface seismic section.

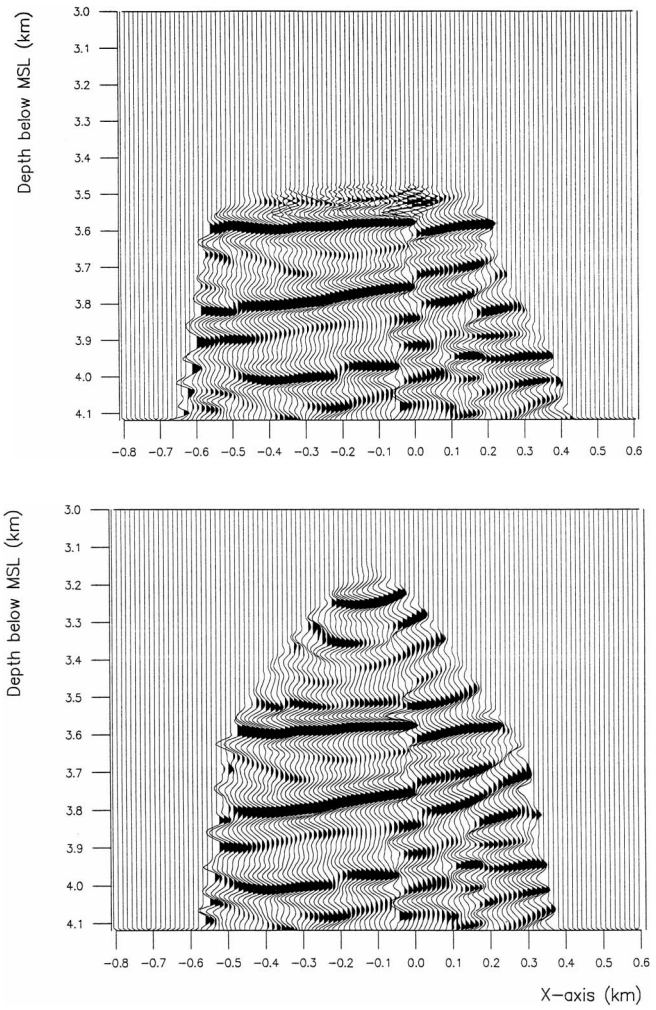

FIG. 8. Acoustic reverse time migration of nine *z*-components.

REFERENCES

Amundsen, L., 1993, Wavenumber-based filtering of marine point-source data: Geophysics, **58**, 1335–1348.

Chen, H.-W., and McMechan, G. A., 1991, 3-D pseudospectral prestack reverse-time migration with application to reverse-VSP data: 61st Ann. Internat. Mtg., Soc. Expl. Geophys., Expanded Abstracts, 1305–1308.

———1992, 3-D prestack depth migration for salt and subsalt structures using reverse-VSP data: J. Seis. Expl. **1**, 281–291.

Claerbout, J. F., 1971, Toward a unified theory of reflector mapping: Geophysics, **36**, 467–481.

Fokkema, J. T., and Van den Berg, P. M., 1990, Removal of surface-related wave phenomena: The marine case: 59th Ann. Internat. Mtg., Soc. Expl. Geophys., Expanded Abstracts, 1689–1692.

Hokstad, K., 1995, Iterative computation of VSP rotation angles: Presented at the 57th Internat. Mtg., Eur. Assn. Geoscientists and Engineers, Expanded Abstracts, B020.

Holberg, O., 1987, Computational aspects of the choice of operator and sampling interval for numerical differentiation in large-scale simulation of wave phenomena: Geophys. Prosp., **35**, 629–655.

Landrø, M., and Sollie, R., 1992, Source signature determination by inversion: Geophysics, **57**, 1633–1640.

Mittet, R., Amundsen, L., and Arntsen, B., 1994, Iterative inversion/migration with complete boundary conditions for the residual misfit field: J. Seis. Expl., **3**, 141–156.

Mittet, R., and Hokstad, K., 1995, Transforming walkaway VSP data into reverse VSP data: Geophysics, **60**, 968–977.

Mittet, R., Hokstad, K., Helgesen, J., and Canadas, G., 1997a, Imaging of offset VSP data with an elastic iterative migration scheme: Geophys. Prosp., **45**, 247–267.

Mittet, R., Holberg, O., Arntsen, B., and Amundsen, L., 1988, Fast finite-difference modeling of 3-D elastic wave propagation:, 58th Ann. Internat. Mtg., Soc. Expl. Geophys., Expanded Abstracts, 1308–1311.

Mittet, R., Landrø, M., Hokstad, K., and Østmo, S. 1997b, A methodology for 3D elastic depth imaging of marine 3D walk-away VSP data: 59th Internat. Mtg., Eur. Assn. Geoscientists and Engineers, Expanded Abstracts, E46.

Mora, P., 1987, Nonlinear 2-D elastic inversion of multi-offset seismic data: Geophysics, **52**, 1211–1228.

Tarantola, A., 1984, Inversion of seismic reflection data in the acoustic approximation: Geophysics, **49**, 1259–1266.

Wapenaar, C. P. A., Herrmann, P., Verschuur, D. J., and Berkhout, A. J., 1990, Decomposition of multicomponent seismic data into primary *P*- and *S*-wave responses: Geophys. Prosp., **38**, 633–661.

Wiggins, J. W., 1988, Attenuation of complex water-bottom multiples by wave-equation-based prediction and subtraction: Geophysics, **53**, 1527–1539.

APPENDIX A

ELASTIC REVERSE TIME MIGRATION SCHEME

We use a reverse time migration algorithm where the imaging principle is based on gradient expressions from nonlinear inversion theory (Mora, 1987; Mittet et al., 1994, 1997a). Depth images are obtained from the gradients of the density and Lamé parameters λ and μ.

The gradients g_ρ, g_λ, and g_μ are defined from the variation of the objective function,

$$J = \frac{1}{2}\int_0^T dt \int dS_g \big[\rho(\mathbf{x}_g)\Delta v_i^2(\mathbf{x}_g, t) + c_{ijkl}(\mathbf{x}_g)\Delta\epsilon_{ij}(\mathbf{x}_g, t)\Delta\epsilon_{kl}(\mathbf{x}_g, t)\big], \qquad \text{(A-1)}$$

where $\Delta\epsilon_{ij}$ and Δv_i are the difference between forward-modeled fields and the measured fields. The surface integral runs over the receiver coordinates. T is the recording time, and c_{ijkl} is Hooke's tensor. In a marine walkaway VSP, displacement velocity is measured. By the reciprocity principle, this is equivalent to a pseudo-pressure $\dot{\Psi}$ measured in a reverse VSP experiment. For this case, the objective function simplifies to

$$J_{WVSP} = \frac{1}{2}\int_0^T dt \int dS_g \frac{1}{M(\mathbf{x}_g)}\Delta\dot{\Psi}^2(\mathbf{x}_g, t), \qquad \text{(A-2)}$$

where M is the bulk modulus of water and $\Delta\dot{\Psi}$ is the residual pseudo-pressure. When we use smooth macromodels without the free surface of the air–water interface, the forward-modeled field contains transmitted energy only. If the modeled first arrivals match the first arrivals in the real data, the residual $\Delta\dot{\Psi}$ is an upgoing field, i.e., the reflections.

The variation of the objective function is

$$\delta J = \int d^3x [g_\rho(\mathbf{x})\delta\rho + g_\lambda(\mathbf{x})\delta\lambda + g_\mu(\mathbf{x})\delta\mu], \qquad \text{(A-3)}$$

where the equations for the gradients are

$$\begin{aligned} g_\rho(\mathbf{x}) &= -\int_0^T dt\big[\partial_t v_i^{\text{mod}}(\mathbf{x}, t)\big]\partial_t \Delta v_i(\mathbf{x}, t), \\ g_\lambda(\mathbf{x}) &= \int_0^T dt\big[\partial_t \epsilon_{ii}^{\text{mod}}(\mathbf{x}, t)\big]\partial_t \Delta\epsilon_{jj}(\mathbf{x}, t), \end{aligned} \qquad \text{(A-4)}$$

and

$$g_\mu(\mathbf{x}) = 2\int_0^T dt\big[\partial_t \epsilon_{ij}^{\text{mod}}(\mathbf{x}, t)\big]\partial_t \Delta\epsilon_{ij}(\mathbf{x}, t).$$

Here, $\epsilon_{ij}^{\text{mod}}$ and v_i^{mod} are forward-modeled strain and displacement velocity fields, and $\Delta\epsilon_{ij}$ and Δv_i are the back-propagated difference between forward-modeled fields and the measured fields. We define the corresponding preconditioned gradients by

$$\hat{g}_\eta(\mathbf{x}) = B(\mathbf{x})g_\eta(\mathbf{x}), \qquad \text{(A-5)}$$

where $\eta = \rho, \lambda$, or μ and $B^{-1}(\mathbf{x})$ is proportional to the average energy of the forward-modeled field in position $\mathbf{x}$. In an inversion scheme, the preconditioning function $B(\mathbf{x})$ is an approximation to the diagonal part of the inverse Hessian tensor. For migration purposes, $B(\mathbf{x})$ can be viewed as a geometrical spreading correction.

The back-propagation of the residual fields is equivalent to reverse time migration of the upgoing reflected wavefield. The imaging condition, computed by correlation of back-propagated (upgoing) and forward-modeled (downgoing) fields, is equivalent to Claerbout's imaging principle. The forward modeling and back-propagation both proceed in the smooth background model where the only spatially localized reflectors are the sea bottom and, if present, the free surface.

The migration images are constructed by displaying the preconditioned gradients. For a multishot experiment, the images are

$$I_\eta(\mathbf{x}) = \mathcal{F}\left\{\sum_s \hat{g}_\eta^s(\mathbf{x})\right\}, \qquad \text{(A-6)}$$

where $\eta = \rho, \lambda$, or $\mu\mathcal{F}$ is a filter, and the sum runs over shots.